Article

Effect of Joule Heating on Cell Viability and Device Reliability

Caffiyar Mohammed Yousuff[a,*], Vineet Tirth[b,c], Mohamed Zackria Ansar B.I[a], Kashif Irshad[d*], Ali Algahtani[b,c], Saiful Islam[e]

  [a] C. Abdul Hakeem College of Engineering and Technology, Melvisharam, India. (CMY)(MZA)(cmd.yousuf@gmail.com, zackriaansarbi@gmail.com)
  [b] Mechanical Engineering Department, College of Engineering, King Khalid University, Abha-61411, Asir, Kingdom of Saudi Arabia (VT, AA) vtirth@kku.edu.sa, alialgahtani@kku.edu.sa
  [c] Research Center for Advanced Materials Science (RCAMS), PO Box 9004, Abha-61413, Asir, Kingdom of Saudi Arabia (VT, AA)
  [d] Center of Research Excellence in Renewable Energy (CoRE-RE), King Fahd University of Petroleum & Minerals, Dhahran, 31261, Kingdom of Saudi Arabia (KI)
  [e] Civil Engineering Department, College of Engineering, King Khalid University, Abha-61411, Asir, Kingdom of Saudi Arabia (SI) sfakrul@kku.edu.sa
  *   Correspondence: kashif.irshad@kfupm.edu.sa (KI); Tel: +966 54 785 4711
                 cmd.yousuf@gmail.com (CMY); Tel: +91 63693 43657

Abstract: The application of electrode-based microfluidic devices in biological entity often imposes a problem due to joule heating. The strong applied potentials or micro channels having narrow cross sections generate undesirable temperature inside the microfluidic channels leading to strong thermal distribution inside the micro channel. When intrinsic distribution of temperature, if not fix with threshold value, causes device damage or cell loss. In this work, we investigate the effects of temperature generated due to joules heating effects and we attempt to address the design constraints for minimizing the joule heating effects in the microfluidic device for developing effective microfluidic device. The device reliability was analyzed under different parametric constraints for various types of substrate materials (PDMS, PMMA, Polyimide and glass). We also attempt to investigate the effects of cell reliability due to strong temperature gradients generated through different applied potentials on different cell types. Furthermore, the response of the device performance due to different electrode configuration and different conductivity of the medium was also studied. Our investigation will eventually provide guidelines for microfluidic researchers to fabricate efficient electrode based microfluidic device which will ultimately help to choose a critical channel dimensions, threshold potentials, and conductivity of solutions in order to avoid device damage and cell loss.

Keywords: cell viability; device reliability; joule heating; eDEP devices.

1. Introduction

When cell sorting is carried out inside the microchannel, often forces is needed to drive the sample flow throughout the microchannel. Electrokinetic phenomenon arises due to the interaction occurring between induced electric charges and external electric field. There exists many electrokinetic methods to control the flow of the sample inside the micro channel, but dielectrophoresis remains superior [1]. Joule heating is often observed in devices which uses electrode to drive the fluid flow. Joule heating arises due to current flow through the buffer solution [2]. This current arises from the applied electric potential on the electrodes inside the microchannel. The interaction of current with the buffer solution has a keen impact on electrical resistance. When an electrical resistance increases, more   heat is dissipated onto the fluid. These results in temperature gradient formation in the fluid present inside the microchannel. The strong electric field gradient generated using Electrode based microfluidic devices has been widely used in bio-medical application for cell trapping[3], for studying cell characteristics [4] and cell

sorting [5]. Behavior of neurons were recorded using an integrated electrode array [6]. Cells like melanoma cells (M2), K562 cells was cultured and tested for viability, cell shipment at different temperature conditions [7]. Shouhui et al. demonstrated that prostate-specific-antigen (PSA) in human serum can be detected using the screen printed electrode [8]. Chen et al. demonstrated that Micro electrodes can effectively be used for separating the polystyrene particles [9].

Joule heating generated inside the microchannel also find application in many ways such as trapping and concentration of cells[10].The joule heating in polymers changes its microstructure and this improves the electrical properties of composite [11].The bio-compatible temperature on electromagnetic based microfluidic device is achieved due to the internal temperature generated due to joule heating [12]. Even though the joule heating has many application as mentioned in above literature, the impact on human cells due to joule heating often leads to lethal injury or cell death [13]. Joule heating in an electro-osmotic flow based microfluidic devices results in deviation of velocity inside the microchannel [14] which results in cell separation failure. The application in which strong electric field density generated inside a microchannel results in higher joule heating effect which denatures the protein components inside the human cells [15]. Furthermore, the effect of joule heating also causes inefficient device performance in application towards cell sorting (lowers separations resolution) [15]. Several DEP based microfluidic devices were studied and experimentally investigated for cell sorting efficiency. It has been investigated that, a typical electrode configuration can generate a strong DEP force at minimal applied voltages for efficient cell separation [16–18]. However, improper design of electrode geometry may also results in strong joule heating effects that eventually destroys the device performance.

In our recent work, we studied the sorting efficiency of red blood cells, white blood cells, platelets, antigen presenting cells and circulating tumor cells using different electrode geometries   using DEP phenomena and optimal device design configuration was found with triangular electrode. This DEP   based cell sorting enables to separate distinct cell types in different collection outlets in a single run which can   be further used for DNA extraction, drug   discovery, high-throughput molecular screening, understanding prognostic information about patients [19]. The electrode geometry has a direct influence in the electric field distribution inside the microchannel [20]. The amount of heat dissipated in the fluid also relies on electrode[21]. The electrode width and electrode height remains responsible in generating the amount of dep force over the human cells.

Certain electrode geometry requires high applied electrode potential for cell sorting. However, an application of high electric field creates strong thermal gradient across the micro channel, especially around the electrode tip, creating strong joule heating region. The cells that exposes in these region will eventually get impacted by high temperature causing cell damages if the threshold temperature exceeds 316.25K [22]. The type of electrode and substrate materials also contributes for generating different field gradient for the applied voltage. In case of DEP based cell sorting application, threshold applied potential is required for effective separation [23–25], however for few electrode materials used in device, the device may generate strong temperature gradient that affects the cell viability when it is flown out at collection outlet [26,27], though separation may be effective [28]. This ultimately shows the device degradability for cell sorting application [29,30].

Numerous attempt has been made to understand the effects of joule heating with respect to cell death and device reliability. Erickson et al. performed combined experimental and numerical analysis of the joule heating and heat transfers at microchannel intersection in polydimethylsiloxane (PDMS) and hybrid PDMS/Glass microfluidic systems [31] and demonstrated that hybrid microfluidic system helps in maintaining the uniform and low buffer temperature. Chein et al. presented analytical model for prediction of pressure and temperature under joule heating effect in microfluidic device [32]. In their study, they observe that, fluid temperature variation is with respect to heat transfer

coefficient of cooling mechanisms. Zhu et al. studied the distribution of temperature on the surface of polymeric chip by using advanced thermograph system [34]. They reported that joule heating produced at high electric field can rise temperature of device above 40°C additionally. It is further observed that, joule heating also affect the flow profile in dielectrophoretic microfilters [33]. Brans et.al. observed the effects of temperature profile on liquid inside a microchannel in which the particle is suspended [35]. The particles are optically trapped to establish the temperature of the surrounding liquid and temperature increase due to Joule heating of the ionic liquid was monitored using their setup. They compared Brownian movement of particles at both room temperature and motion of microparticles when the power remains dissipated inside the microfluidic system and provided the estimate of temperature increase inside the microchannel. In application towards cell sorting and isolation, the collection of healthy cell after the cell sorting mechanism tends to offer a wide range of scope in the field of DNA extraction, drug discovery and cell culture. Most of the reported literature shows that, the system either requires high voltage for cell separation resulting in joule heating effect or complicated design constraints [3,36,37]. Application of higher voltages on the microfluidic device also damages the microchannel hindering its application for multiple runs.

All the above literature has highlighted the investigation on the joule heating on the device or the factors which contributes joule heating effects. In order to develop an efficient and reliable microfluidic device to avoid cell damages in the presence of joule heating needs to be critically addressed in all electrode-based DEP devices. Rise in device temperature is often observed in all electrode based DEP system resulting in cell death, separation failure which makes the device non-reliable for downstream analysis. All eDEP based devices produces joule heating resulting in increased temperature gradient inside a microchannel when design constraints not considered properly. Therefore, the device experiences larger unusual temperature leaving the cells damaged.

All these issues can be overcome by selecting proper electrode geometry, electrode potentials and choosing proper substrate materials which will eventually causes low thermal effects inside the devices and avoids the issues of cell damage/loss and provides reliable device performance. It is further noted that, the conductivity of the medium also has significant impact on joule heating inside a microchannel when the applied voltage exceeds above the threshold value [38]. Therefore, in this research, we attempt to explore the effect of various parameters including applied potential, electrode geometry, substrate materials and conductivity of the medium which can provide optimal solution to avoid joule heating effects thereby improving device performance, reliability and avoiding cell loss.

We observed the effects of temperature on the cell when it is exposed to the region of strong thermal gradient at various positions in a microchannel (initial, center and rear end). The thermal impact on cells and its survival time gives us a clear idea about cell viability. Our study reveals the maximum temperature a cell can withstand inside a micro channel to remain viable and maximum voltages that can be applied to the device for effective DEP based cell separation under various parametric constraints. We attempt to evaluate the device performance by tweaking around various geometrical parameters including electrode geometry, substrate materials, applied potentials and medium conductivity. An effective and optimum design solution is derived from our study that will enable the future researchers to design and develop reliable DEP devices and other electrode based microfluidic devices for various bio clinical applications.

2. Materials and Methods

2.1. Theory of DEP and Joule heating

The Movement of uncharged particle under the region of non-uniform electric field constitutes a force termed as 'Dielectrophoresis'. Under this condition, each particle will have different coulombic force at both ends which give rise to electrokinetic flow

movement due to net force imbalance. The DEP force of the spherical particles is expressed as [39] ,

$$F_{DEP(i)} = 2\pi\varepsilon_0\varepsilon_m Re[f_{CM}(\omega)]\ R^3\ \nabla E^2 \tag{1}$$

Where 'ε_m' is the relative permittivity of the suspending medium, R is the radius of the particle, ∇E^2 denotes gradient of the electric field, $Re[f_{CM}(\omega)$ denotes the real part of the Claussius Mosotti [CM] factor that determines effective polarisability and is expressed as[40] ,

$$f_{CM}(\tilde{\varepsilon}_p, \tilde{\varepsilon}_m) = \frac{\tilde{\varepsilon}_p - \tilde{\varepsilon}_m}{\tilde{\varepsilon}_p + 2\tilde{\varepsilon}_m} \tag{2}$$

Where $\tilde{\varepsilon}$ is the complex permittivity and defined as,

$$\tilde{\varepsilon} = \varepsilon - j\left(\frac{\sigma}{\omega}\right) \tag{3}$$

Therefore, CM factor can be written as,

$$f_{CM}(\varepsilon_p, \sigma_p, \varepsilon_m, \sigma_m, \omega) = \frac{(\varepsilon_p - \varepsilon_m) + j/\omega(\sigma_p - \sigma_m)}{(\varepsilon_p + 2\varepsilon_m) + j/\omega(\sigma_p + 2\sigma_m)} \tag{4}$$

The CM factor is dependent on the complex permittivities of the particles and the suspending medium. When the suspending medium is less polarizable than the particles are attracted to the higher field region commonly referred as positive dielectrophoresis (pDEP), in contrast, when the suspending medium is more polarizable consequently the particles are repelled from the region of higher electric field, this give rise to negative dielectrophoresis (nDEP).

If 'σ' is the conductivity of the buffer solution between the positive and negative electrode then the heating power per volume V depends linearly to conductivity of the suspending medium (σ) and to the square of the electric field strength and is expressed as [41] ,

$$q = \frac{P_{heat}}{V} = \sigma \cdot E_{rms}^2 \ \propto \ \sigma \cdot U_{rms}^2 \tag{5}$$

Where 'rms' denotes root mean square value, 'U' represents the voltage applied between the electrodes. The amount of heat generated (P_{heat}) is equal to the amount of heat dissipated under the steady state condition [2]. The Electric field (E_{rms}) depends on the conductivity of the suspending medium (σ) which is greatly affected by the change in temperature and is expressed as ,

$$\sigma = \sigma_0[1 + \alpha(T - T_0)] \tag{6}$$

Here, 'σ_0' refers to the conductivity at a reference temperature T_0, and α is the temperature coefficient of the suspending medium. The Joule heating-induced temperature field is governed by the energy equation expressed as [42] ,

$$\rho C_p\left(\frac{\partial T}{\partial t} + \overrightarrow{u_B}\ \nabla T\right) = k_1\nabla^2 T + \lambda(T)(\nabla\phi)^2 \tag{7}$$

where C_P and k_l represents the specific heat and thermal conductivity of the buffer solution, respectively, and they are considered to be constant (i.e., independent of temperature).

2.2. Geometry of the Microfluidic chip

The three dimensional microfluidic chip is shown in Figure (1). Device consists of cells mimicking human WBC, APCs and CTCs in the size range of 15 μm [43]. Under the application of DEP force each cells experiences different dep forces [18]. Electric potential is applied on top and bottom of device for generating non-uniform electric field. +V is applied on the bottom of the device illustrated in Figure 1(b) and -V is applied on the top of the device as shown in Figure 1(c). The device has a channel length of 1400 μm and channel width of 300 μm. The electrolyte used is PBS solution in the ratio of 1:9 to the blood was used throughout the simulation. The device has a thickness of 60 μm as seen in Figure (1d).
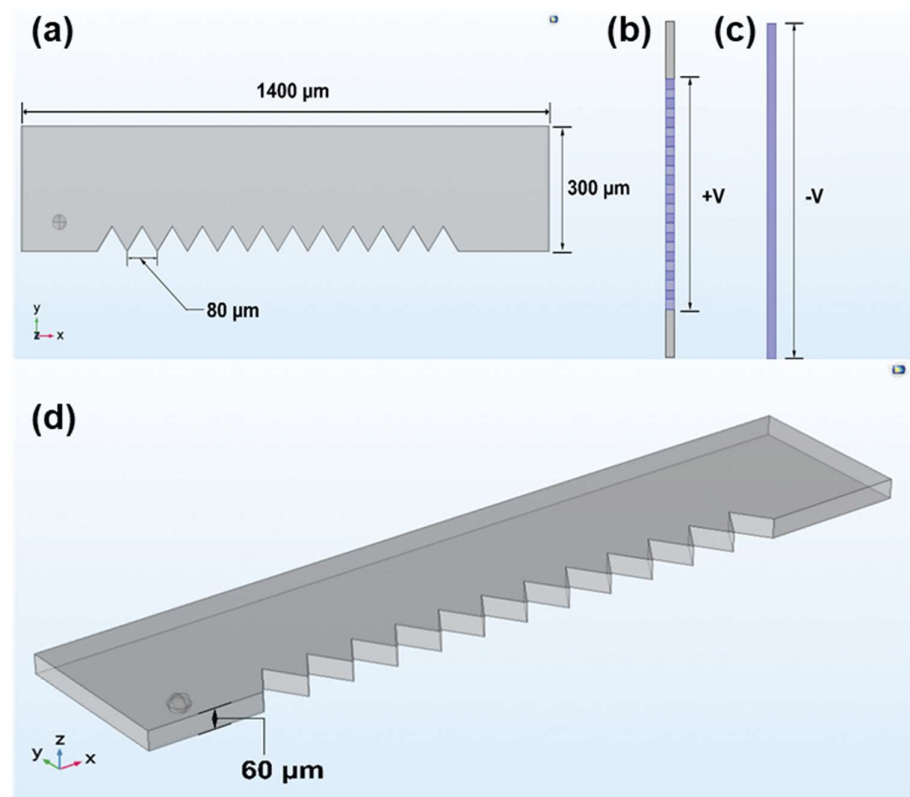

Figure 1. (a) Three dimensional microfluidic device design represented in XY axis orientation. (b) Bottom view of triangular electrode +V applied. (c) Top view of the electrode with -V electrode. (d) An intermediate view representing thickness of the microfluidic device.

2.3. Numerical Analysis :

By using COMSOL Multiphysics software (COMSOL v5.3a), a three dimensional simulation model was created in order to characterize the cell viability and device reliability. Three dimensional model was developed as 2D model failed to show the distribution of temperature in the thickness of the microfluidic chip and around the surface of the cells. Electric field profile is simulated using electric current model. Temperature distribution on the cells caused due to joules heating effect is simulated using bio-heat transfer

model is used. These interfaces were used sequentially to model the problem numerically and detailed description on these interfaces are listed below.

(i) Electric current interface is used in simulation in order to generate non-uniform electric field within the microchannel. The applied electric potentials are regulated by Laplace's equation, given by E= ∇φ. The electrodes are arranged adjacently to the channels wall and are provided with the applied voltages +V and -V   on the top of the microchannel. The rest of the domain inside the model are insulated.

(ii) Bio-heat transfer interface in simulation is used to generate the thermal distribution on the blood cells which submerged with the Phosphate buffer solution for effective isolation. In order to solve energy equation the outer boundaries were set to room temperature of 290 K. The interface provides joules heating effect (i.e., the thermal exposure over the cell caused due to heat dissipated on the solution). The heat transfer equation (7) governs the different temperature distribution inside the microchannel.

(iii) The geometry is meshed with free tetrahedral with minimum size element of 0.18 μm and maximum size element of 50 μm and for the discretization of 62238 mesh elements. A time dependent solver is used to solve electric field and thermal distribution resulted through joules heating simultaneously. The three dimensional geometry and its electrode is defined under the graphic section window.

3. Results

The cells are subjected to different region where it experiences different amount of dep force. The cell path from the initial separation to the final collection outlet has been listed in Figure (2). The three various region of measurement of thermal effects on the cells include initial region (near by the inlets) at a channel length of 100 μm and channel width of 30 μm. The next is the centre region (between the electrodes) at a channel length of 700 μm and channel width of 200 μm. The   final region is nearer to outlets at channel length of 1300 μm and channel width of 240 μm . Each of the cells have distinct cell size. However, all these cells will receive equal amount of thermal effects since they are kept consistent in all the three region. Consequently, a single cell is used for the complete simulation. The region of measurement provides valuable insight about whether the cells remains healthy or exposed to unusual temperature which results in cell destruction or cell dead. Amount of temperature exposed on the cells due to buffer conductivity , electrode shape, substrate material, various metal electrodes was analysed and discussed in below subsections.
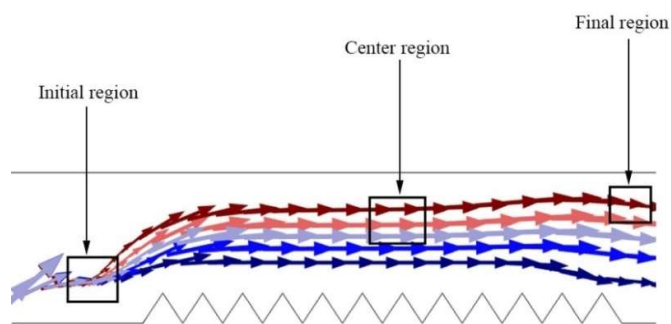

Figure 2. Shows the measurement region inside the microchannel on the particle tracks towards the outlet

3.1. Effect of Buffer Conductivity:

The effect of buffer conductivity on various Cells were analysed. The different cell types exerts same amount of temperature throughout the simulation while the threshold temperature for individual cell types differs accordingly. For the human cells

the damage occurs at 316.5 K [22]. The amount of cell damage is proportional to time it is exposed[44]. Buffer conductivity ranging from 10[mS/m] to 100 [mS/m] was used in order to evaluate the amount of temperature exerted on the cells. The region is classified as initial position, centre position (region with high electric field density) and final region (near to outlets).This region also refer to the tracks which it follow to reach their corresponding collection bins[18]. When the cells are at the initial position as seen in Figure 3(a) with a buffer conductivity of 10[mS/m] the temperature exerted over the cells is found to be 300.14 K at an applied electrode potential of 5Vpp. Under the same applied voltage, when a buffer conductivity is increased to 30 [mS/m] for the same position of the cell, the temperature exerted over the cell is found to be 305.14K as shown in Figure 3(b). With further increase in buffer conductivity of 55 [mS/m] the temperature exerted over the cells get raised to 310.38K .Further increase in buffer conductivity to 100 [mS/m], the temperature of 326.23K is generated over the cells as shown in Figure 3(c). The cells were tested at 10V with different buffer conductivity as shown in Figure 3(d), buffer conductivity from the range (10-100mS/m) was tested at 15V as shown in Figure 3(e). Maintaining 25V with different buffer conductivity is shown in Figure 3(f). All these plot demonstrates that temperature increases with the increase in buffer conductivity at a constant applied potential. The temperature above 316.5K on the cells will often lead to cell damage leading to the cell death if they are analysed over a long period of time as stated in [45–47]. The second phase of simulation deals with same range of buffer conductivity from (10 - 100 [mS/m]) at the channel length of   700 μm and channel width of 200 μm.

As these region is nearer to the electrode, the distribution of non-uniform electric field is greater compared to that of the other region. Nevertheless, the cells passing through these region is intended to have more thermal effects. This condition exhibits larger thermal values as the applied potential directly influence the buffer solution since it is nearer to the electrode. The temperature exerted by the cell is found to be gradually increasing from 311.41K to 325.58K with an increase in buffer conductivity. The buffer conductivity of 10 [mS/m]   and 30 [mS/m] is considered to be safer with a least cellular damage. While increasing buffer conductivity from these range causes irreversible cellular damage leading to cell death as it exceeds the threshold temperature of the cells. The final phase of the simulation was carried out for the same range of buffer conductivity nearer to the collection outlet bins. The cell was positioned at the channel length of 1300 μm and channel width of 220 μm. The cells making their way from previous region enters these region later on collected at the outlet as indicated in [18,48]. Thermal effects tend to be low at this region of the device ranging from 295.32K to 311.41K as shown in Figure 3(a). The healthy cells entering this region never suffer any lethal injury or cell death throughout the buffer conductivity ranging from 10 to 100 [mS/m]. This detailed result provides guidelines on cell viability.
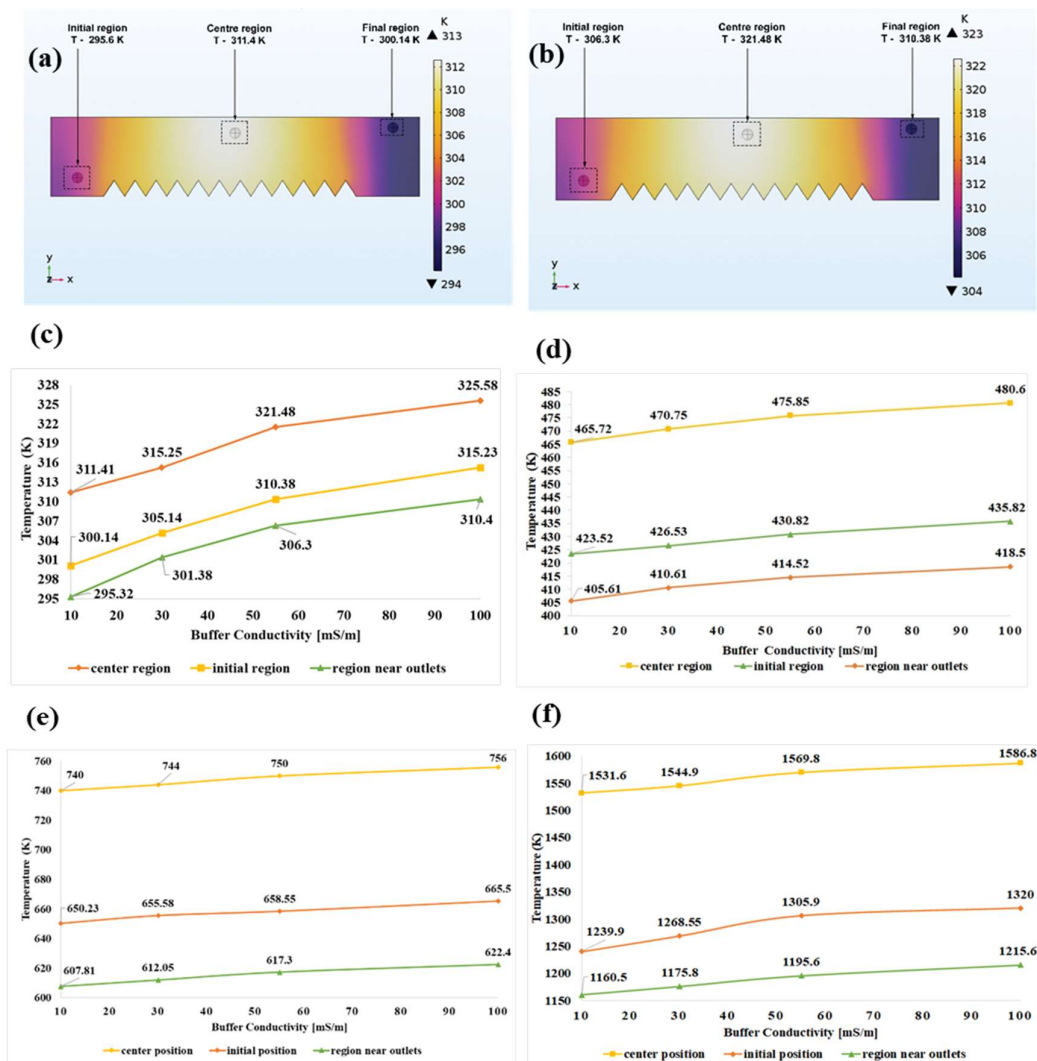
Figure 3. (a) Temperature exerted by cells in all three region with buffer conductivity 10 mS/m. (b) Temperature exerted by cells in all three region with buffer conductivity 55 mS/m. (c) Response of different buffer conductivity at three region with a constant applied potential of 5V. (d) Response of different buffer conductivity at three region with a constant applied potential of 10V. (e) Response of different buffer conductivity at three region with a constant applied potential of 15V. (f) Response of different buffer conductivity at three region with a constant applied potential of 25V.

3.2. Effects of Applied Electric Potential

The Applied electrode potential was studied for the device reliability and cell reliability. The heat energy generated due to joule heating is directly proportional to the square of the electric field applied [49]. The applied potential in simulation are 5V , 10V, 15V, 25V, 40V. Under applied potential of 5V, the cells were found to be healthy and viable as the threshold temperature does not exceeds more than 316.25 K as shown in Figure 4(a). The electric field at the three region is different, as a result thermal distribution in each of these region is unique. When the applied potential is increased to 10V, the cells exerts temperature more than 400 K . With the further increase in voltage to 15V, the cells exerts temperature more than 600 K as shown in Figure 4 (b). Complete cell separation can be easily achieved at the time period of 0.5 to 1 second   [50].   Distribution of applied electric potential inside the channel of 300 µm is shown in Figure 4(c). The time at which the cell reaches it threshold temperature level is found to be 1.45 seconds when 5V ap-

plied as shown in Figure 4(d). Hence the cells remain viable for long time in this case. Further increase in applied potential to 10V time gets reduced to 0.3 seconds as shown in Figure 4(e). Inference with respect to threshold temperature is listed in Table 1.

Table 1. Time required to reach threshold temperature at different electric potential.

Applied Electrode Potential	Time to reach threshold Temperture 316.25 K (in seconds)	Inference
5	1.45	Effective cell separation with maximum cell viability
10	0.3	Cell Separation leading to cell death
15	0.15	Cell Separation leading to cell death
25	0.04	Cell Separation leading to cell death
40	<0.01	Cell death occurs at initial region itself

With the further increase in voltage to 25V the temperature gets raised to 2500K at this stage irreversible cellular damage occurs. When the voltage is further increased to 40V the temperature exceeds above 2000K. There is a steady increase in temperature with respect to the applied electric potential as shown in Figure 4(f). The temperature received by human cells in all three region under different applied electrode potential is listed in below tables.

The impact of applied electric potential on cell viability was analysed in all the three regions. The initial region (near to inlet) receives less temperature than the centre region. The thermal distribution on the cells at different applied electric potential in initial region is listed in table (1). We varied the applied potential from the range of 5V to 40V. It is found that the region receives minimum temperature of 301K under the application of 5V maintaining the cell viability until the cell gets deposited on the outlet bins. The further increase in applied potential to 10V drastically increases the temperature to 424K decreasing the survival time of the cells. The temperature of 651K and 1240K are distributed in this region at 15V and 25V. Even though, the cells has shorter survival period these cells reaching the outlet are not viable. With the further increase in applied electric potential the viability of the cells further reduces resulting in cell death.

Table 2. Temperature exerted by cell at initial region at different electric potential.

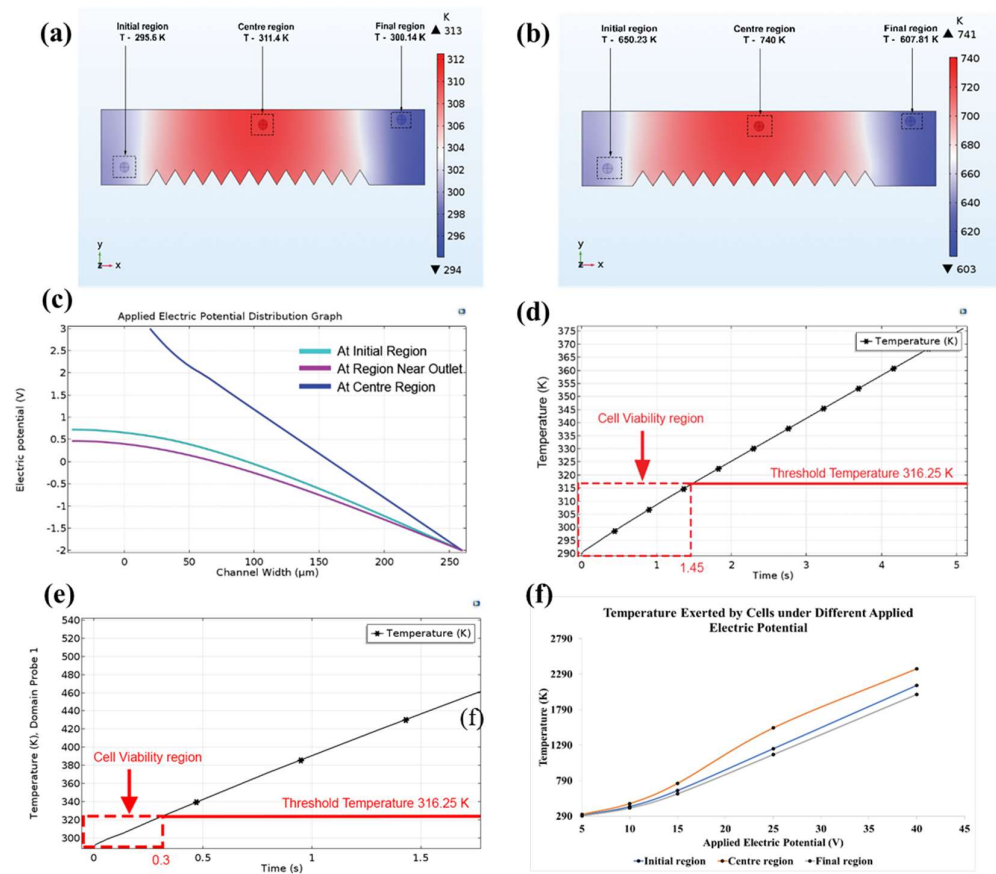| Applied Electrode Potential	Cell Viability)	Temperature exerted at initial region (in kelvin)
5	100% Viable	301
10	Viable till 0.3 seconds	424
15	lethal injury, Cell death	651
25	lethal injury, Cell death	1240
40	lethal injury, Cell death	2132

Figure 3. (a) Temperature distribution in different region at 5V. (b) Temperature distribution in different region at 15V. (c) Potential distribution at three regions at 5V (d) Threshold temperature plot for 5V. (e) Threshold temperature plot for 10V. (f) Temperature exerted by cell at different applied electric potential.

The impact of applied electric potential on cell viability was analysed in all the three regions. The initial region (near to inlet) receives less temperature than the centre region. The thermal distribution on the cells at different applied electric potential in initial region is listed in table (1). We varied the applied potential from the range of 5V to 40V. It is found that the region receives minimum temperature of 301K under the application of 5V maintaining the cell viability until the cell gets deposited on the outlet bins. The further increase in applied potential to 10V drastically increases the temperature to 424K decreasing the survival time of the cells. The temperature of 651K and 1240K are distributed in this region at 15V and 25V. Even though, the cells has shorter survival period these cells reaching the outlet are not viable. With the further increase in applied electric potential the viability of the cells further reduces resulting in cell death.

The centre region of the device has high thermal distribution and has great impact on the cells. The temperature in this region is listed in table (3). It is noted that, the major difference of around 10K to 15K is found between this region and to the region near the inlet. The region exhibits minimum temperature of 313K under the applied electric potential of 5V. With further increase of applied potential to 10V, the temperature recorded in this region is found to be 466K, where the cell suffers lethal injury. However, if these cells remain for quiet longer period may result in cell death. Furthermore, when the applied potential is raised to 15V, 25V, 40V may subsequently increase the region temperature beyond 750K, 1500K, 2300K leading to irreversible cellular damage as the temperature on the cells exceeds far beyond its threshold limit.

Table 3. Temperature exerted by cell at centre region at different electric potential.

Applied Electric Potential	Cell Viability	Temperature exerted at Centre region (in kelvin)
5	100% Viable	313
10	Suffers lethal injury	466
15	lethal injury, Cell death	752
25	lethal injury, Cell death	1533
40	lethal injury, Cell death	2367

Final region (near to the outlet) receives lowest thermal gradient. As a result the cells entering in this region are subjected to low thermal effects compared to other regions. Under applied potential of 5V, the temperature in this region is found to be 294K establishing safer temperature zone for the cells to be viable. These cells remains healthy at the outlet bins. At 10V, the region has minimum temperature of 404K leading the cells to undergo lethal injury. With a further increase to 15V, 25V, and 40V the temperature in this region drastically increases to 606.5K, 1158K, 2005K resulting in cell death.

Table 4. Temperature exerted by cell at final region at different electric potential.

Applied Electric Potential	Cell Viability	Temperature exerted at Final region (in kelvin)
5	100% Viable	294
10	Suffers lethal injury	404
15	lethal injury, Cell death	606.5
25	lethal injury, Cell death	1158
40	lethal injury, Cell death	2005

When the applied electric potential is increased the cell viability gets reduced as they are exposed to high thermal effect. Irrespective of the time period it is exposed to it. Selection of applied electric potential directly influences thermal impact on the cells. The temperature exposure offers a consistent understanding of cell viability. However, the applied potential of 5V to the device results in 100% viability of the cells.

3.3. Effect of Electrode material

Material such as Gold, copper, silver, nickel, platinum and aluminium are mainly used as electrode in microfluidic devices [51]. The parameters including electrical conductivity, coefficient of thermal expansion, density and thermal conductivity is modelled accordingly and listed in table (5) . All the materials were chosen from COMSOL Multiphysics library. The thermal effect on the cells for cell viability was tested and temperature generated in device using these material was contrasted for device reliability. The distribution of temperature varies accordingly with the region. The minimum temperature exerted by the device is shown in Figure 5(c). Copper exerts lowest temperature of 294 K on the device. Platinum and Gold exerts temperature of 315 K and 314.8 K which is recorded has maximum temperature under the applied electric potential 5V. The maximum temperature exposed by the various material is shown in Figure 5(d).   The applied electrode potential of 5 V was initially kept throughout the simulation. The temperature generated on the cells varies from one material to another.

Table 5. Material properties of various metal electrodes

Electrode material	Electrical conductivity [S/m]	Coefficient of thermal expansion [1/K]
Aluminium	35.5e6	23.1e-6
Gold	45.6e6	14.2e-6
Copper	58.1e6	16.5e-6
Silver	61.6e6	18.9e-6
Nickel	13.8e6	8.80e-6
Platinum	8.9e6	8.80e-6
Aluminium	35.5e6	23.1e-6

The commonly used electrodes in microfluidics include platinum, gold due to its inertness, conductivity and malleability. All the material was tested under the same applied electric potential. The temperature exerted by the cells using copper electrode is shown in Figure 5(a). Temperature exerted due to platinum electrode is shown in Figure 5(b). Gold and platinum resulted a temperature rise of approximately 1 to 1.5 kelvin relative to other materials. Gold and platinum electrode recorded highest thermal effect on the cells with temperature of 312.80 K and 313.5 K at the centre region. At the region near the outlets the temperature on the cells due to this electrode was found to be 297.85 K and 299.5 K. Even though, these material has unique withstanding property at higher temperature. The cost makes it undesirable for many applications. If a cell is meant to be exposed to the greater time period, then these materials are highly suitable for their toughness. Aluminium and lithium confronts the temperature of 301.19 K and 301.30 K at initial region. While copper and silver electrode experienced very low temperature at initial region as much as 300.14 K and 300.50 K but at the centre region the copper exposes the temperature as high as 311.41K and silver exposes the temperature of 311.6 K. The comparative plot of temperature exerted by cell by different electrode material is shown in Figure 5(e). This temperature remains safer for the cell in preventing them from cell injury or cell death. At the region near outlet, copper material exposes the temperature of 295.32 K on the cells while silver results with 296.02 K temperature on the device.

Table 6: Temperature exerted by cell in all three region at applied electric potential of 10 V using different electrode materials

Applied Electrode potential	Electrode material	Temperature Exerted in Initial region (in kelvin)	Temperature Exerted in centre region (in kelvin)	Temperature Exerted in Final region (in kelvin)
10	Gold	425.13	417.8	406.75
10	Copper	423.52	416.41	405.61
10	Silver	423.88	416.6	405.95
10	Nickel	425.53	417.4	407.35
10	Platinum	426.48	418.7	408.20
10	Aluminium	424.57	417.56	406.19
10	Lithium	424.68	417.27	406.3

The thermal distribution in all the three region using different electrode material is listed in table (6).It is noted that, copper produces least temperature distribution of around 405.61 K while the use of platinum electrode material results increased temperature distribution of 408.20K. Major variation of 1K to 2.5K is noted in material like gold, nickel, platinum , aluminium, lithium compared to copper electrode . This material are often employed when there is need for multiple runs.
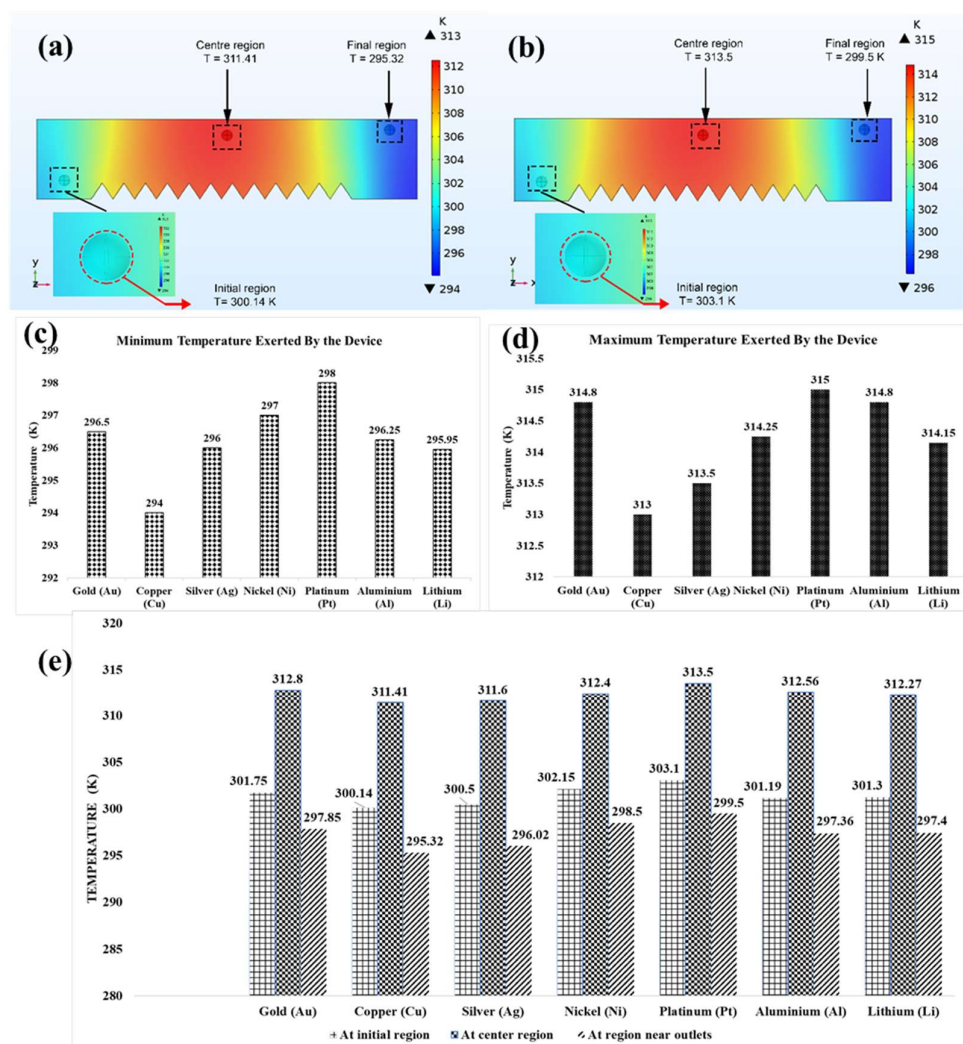

Figure 5. (a) Thermal effects on cell due to copper electrode. (b) Thermal effects on cell due to platinum electrode. (c) Minimum temperature plot of different electrode material on device. (d) Maximum temperature plot of different electrode material on device.

Aluminium and lithium exposes the temperature of 312.6K and 312.27K in the centre region and at the region near the outlets the cell gets experienced to the temperature of 297.36K and 297.4K. However, when lithium reacts with organic solvent (PBS solution) for long period of time it becomes thermally unstable [52]. Nickel records the temperature of 298.5K at the region near the outlets and higher temperature of 312.4K at centre region. The thermal effect on the cell at this voltage will often result in lethal injury, when further increased to 25V and 40V, the reliability of the device is weakened as the temperature increases closer to its boiling point. The use of both copper and silver is highly preferable in this case making it a suitable material for low-cost microfluidic device manufacturing.

3.4. Effect of substrate material

The impact of technologically important substrate material on the cell of interest was examined. Glass is mainly used in microfluidics for its beneficial optical characteristics, stability[53]. Heat distribution in glass remains uniform unlike any other substrate material[54] . It is noted that the substrate material which has high thermal conductivity are more likely to damage the cells.   The cells were analysed on all the three regions. Substrate material like PDMS (polydimethylsiloxane), PMMA (Polymethylmethacrylate), polyimide, glass was analysed using the simulation. Material properties of each of the substrate has been listed in the below table (7).

Table 7: Material properties of substrate material

| Parameters	PDMS	PMMA	Polyimide	Glass
Thermal Conductivity[1,2][W/(m·K)]	0.16	0.19	0.15	0.8
Electrical conductivity[3][S/m]	0.25	0.25	0.5	0.5
Density[4–6] [kg/m³]	970	1190	1300	2329
Relative permittivity	2.75	3.0	1	11.7
Heat capacity at constant temperature [J/(kg·K)]	1460	1420	1100	700
Youngs modulus [Pa]	750e2	3e9	3.1e9	170e9
Poisson's ratio	0.49	0.40	1	0.28
Coefficient of thermal expansion[1/K]	9e-4	70e-6	9e-6	2.6e-6
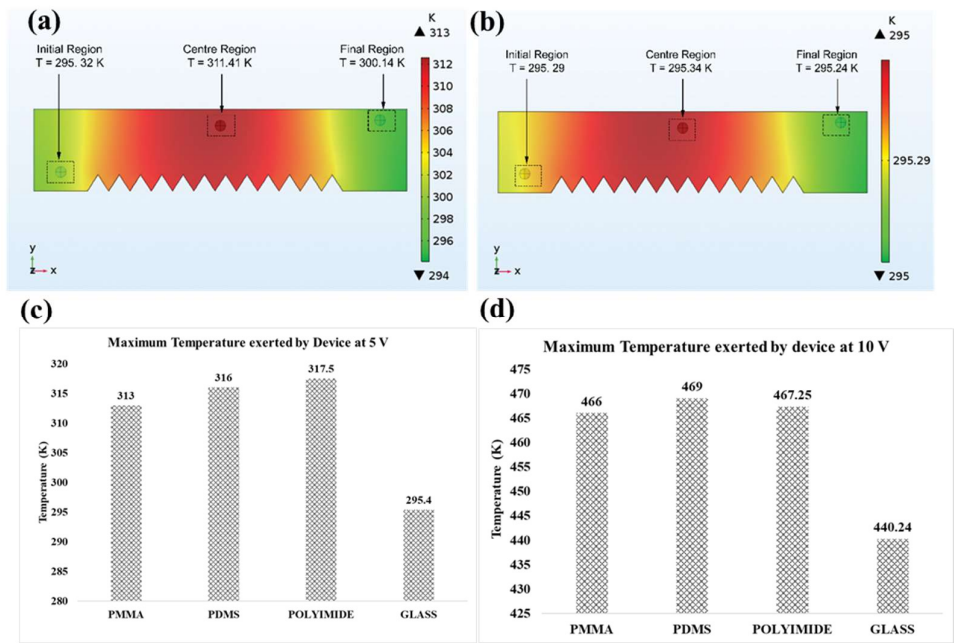
Figure 6.(a) Thermal effects on cells at 5V using PMMA material. (b) Thermal effects on cells at 5V using glass material. (c) Maximum temperature exerted on the device at 5 V. (d) Maximum temperature exerted on the device at 10 V

The thermal effect on the cell using PMMA material is shown in Figure 6(a). At the initial region the cells gets exposed to the temperature of 295.32K and 311.41K is exerted at centre region. In the region near the outlet the temperature exerted is 300.14K. The temperature exerted by cells using glass substrate material is found to be in the range of

295.24K to 295.34K as shown in Figure 6(b). Under 5V, all these material exerted the thermal effects within the threshold limit of 330K. The cells undergoes lethal injury when it is exposed to temperature more than 316.25K. PDMS material generated minimal temperature of 316K. Use of PDMS is restricted for prolonged cell separation as it is high hydrophobicity can absorb some bio molecules [61]. Aging of these material also changes its mechanical properties yielding biased results [62].

Polyimide exerts the temperature of 297.15 K at the region near the outlet and 302.82 K at the initial region. The temperature exerted at the centre region is found to be 314.71 K. The temperature exerted due to different substrate material at 5 V is shown in Figure 6(c). The maximum temperature more than 440 K is exerted on the device due to different substrate material at 10 V is shown in Figure 6(d). Polyimide serves an emerging substrate material with high chemical resistance, much biocompatible with high dielectric constant[63,64]. However, these substrate material is not suitable for commercial purpose as it has low impact strength and remains expensive. PMMA is less expensive, more rigid ,has compatibility to many biological application[65].

3.5.Effect of Electrode Geometry

The thermal effects generated by different electrode shape was examined for device reliability. In an DEP based microfluidic devices, electrode geometry plays a vital role in producing non-uniform electric field as gradient of electric field influences the DEP performance[40]. Various electrode shape like square, triangle, rectangle, rectangle with soft edges and square with soft edges was examined.
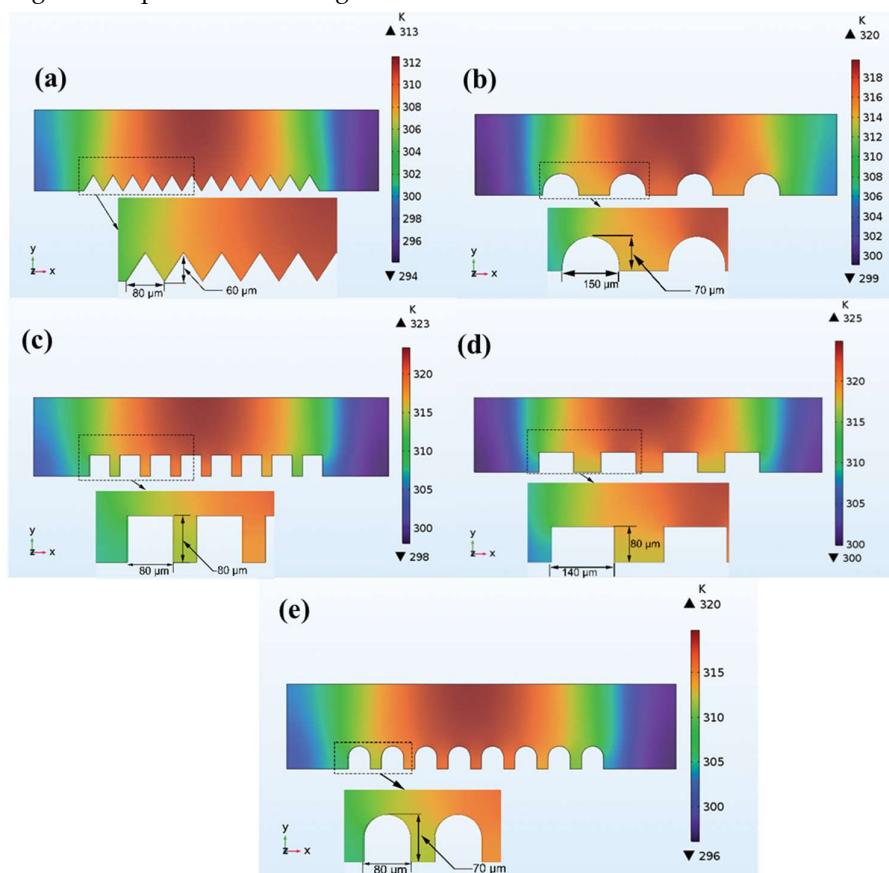

Figure 7. Dimension of various electrode geometry. (a) triangular shaped electrode (b) rectangle with soft edges electrode. (c) rectangle shaped electrode. (d) square shaped electrode. (e) square shaped with soft edges electrode.

Triangular shaped electrode has height of 60 μm and width of 80 μm as shown in Figure 7(a). Rectangle with soft edges has height of 70 μm and width of 150 μm while rectangle shaped is of 140 μm width and 80 μm height represented in Figure 7(b) and Figure 7(c). Square shaped electrode is of 80 μm height and width and Square shaped electrode with soft edges is of 80 μm width and 70 μm height as shown in Figure 7(d) and Figure 7(e). The edges are carved with the radius of 40 μm.   Electrode geometry not only helps in regulating strength of non-uniform electric field but also to facilitate fabrication.

The thermal effects on both cell and to the device due to the electrode geometry will be different. We investigated temperature generated on the device on all the three regions. The temperature at the region near to outlet (final region) received a low temperature, the triangular shaped electrode exploits very low temperature as much as 294 K on the device. While square shaped electrode exposed a temperature of   298 K while square shaped with soft edge exposed a temperature of 296K. Rectangular shaped electrode exerted temperature of 300K compared to all other electrode geometry. Rectangular with soft edges exerts temperature of 299K. At initial region   temperature of 295.32K is exposed with triangular electrode. Square shape and square shaped with soft edged electrode exerts the temperature of 297.23K and 299.95K. While rectangle and rectangular shaped electrode result with temperature rise of 301.24K and 302.25K.

Table 8. Temperature generated across the three region on different electrode geometry with applied electric potential of 10V.

Electrode Geometry	Minimum temperature on the device (at near the outlet) (in kelvin)	Maximum temperature on the device (At center region) (in kelvin)	Temperature at initial region (in kelvin)
Triangular	405.61	465.72	423.52
Square shaped with soft edges	407.53	468.25	425.25
Square shaped	410.56	472.32	426.50
Rectangle with soft edges	412.10	474.25	428.35
Rectangle shaped	413.36	478.05	431.25

Compared to other region, the cell has a high temperature in the centre region. The maximum temperature of 322.25K received by the cell is with rectangle shaped electrode. The cell undergo lethal injury as it exceeds threshold temperature. The triangular electrode exposes the temperature of 311.4K on the cells , however the cells remains viable. The square shaped with soft edges and rectangle shaped with edges electrode exerts temperature of 314.50K and 318.25K on the cells. In this case, the cell remains remain viable with square shaped with soft edges. Triangular electrode has a single sharp edge that concentrates a strong electrical field only at that location. The tip and dimension the electrode   causes strong gradient in non-uniform electric field[66]. Thus, each electrode shape will have distinct region of electric field. As a result, the dimension of square shaped and rectangle shaped electrode results in strong gradient of electric field compared to other electrode geometry. The temperature exerted by the cell at different region at applied electric potential of 10V is listed in table (8).   In order to check device reliability the electrodes were tested under with 5V,10V, 15V, 25V, 40V. The maximum temperature exerted by the electrode is shown in Figure 8. The thermal effects generated using triangular electrode never impacts injury on the cells when analysed at 5V.
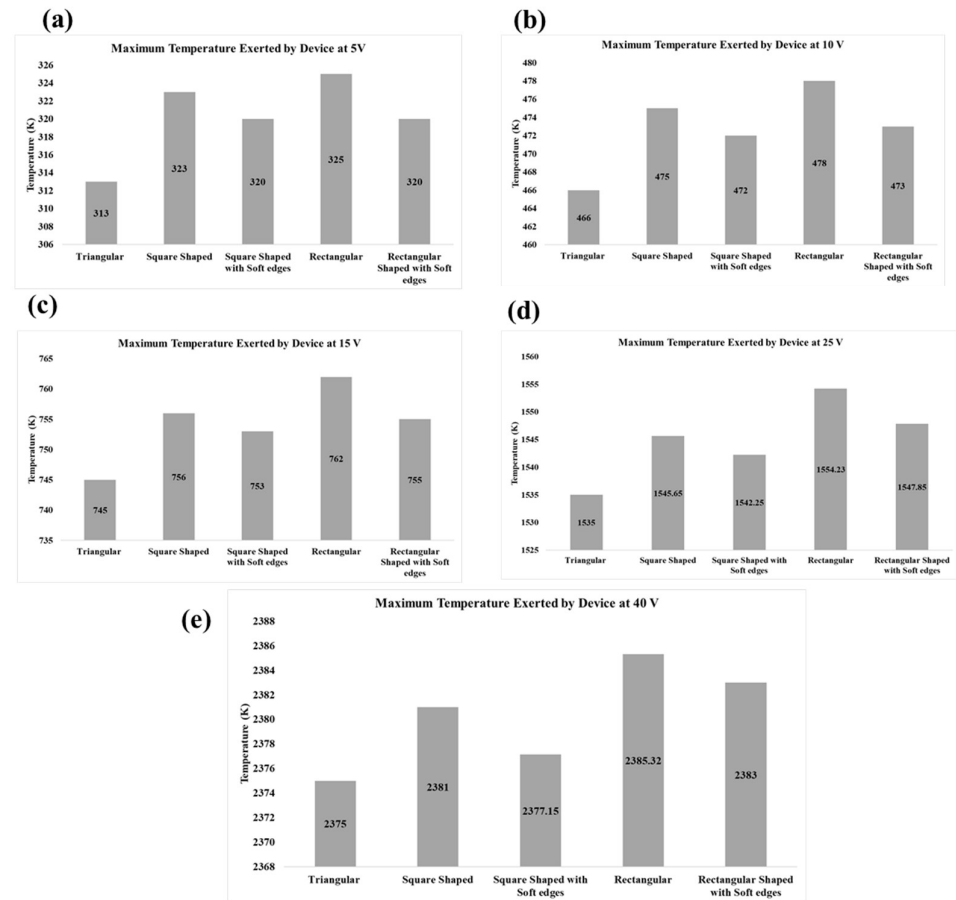
Figure 8. Maximum temperature exerted on the device (a) at applied electric potential of 5V. (b) at applied electric potential of 10V. (c) at applied electric potential of 15V. (d) at applied electric potential of 25V. (e) at applied electric potential of 40V.

In all cases when the applied voltage is varied accordingly, the thermal effect on the triangular electrode is low compared to other electrode. This makes it suitable electrode for fabrication of device. While other electrode at the same applied potential results in increase of temperature of about 10K to 15K compared to triangular electrode. This makes it reliable compared to all other electrode geometry.

4. Conclusion

This papers illustrates the thermal exposure on the cells and device due to joule heating in an electrode based dielectrophoretic devices. Thermal variation generated by using different parameters like electrode material, electrode geometry, substrate material, buffer conductivity of the medium, applied electric potential was investigated at room temperature. Minimum temperature distribution is found at the outlet region whereas, the maximum temperature distribution occurs at the region of strong thermal gradient (in center region). The cells remains viable to the maximum time of 1.45 seconds with buffer conductivity of 10 [mS/m] with 5V which is quiet enough for trapping healthy cells in the outlet bins in an microfluidic device.   However, survival time of the cells inside the microchannel was found to be decreasing with the increase in applied electric potential with buffer conductivity in the range of 10[mS/m] to 55[mS/m]. Furthermore, the increase in buffer conductivity also contributes increased joule heating that eventually leads to more heat generated on the cells that may cause cell death.   In our case study for

DEP based cell separation application, we observed that, the device material fabricated using PMMA substrate and electrode with triangular geometry arrangements are potential to generate least amount of joule heating compare to other electrode arrangements resulting in perfect separation of cells ensuring the cells remains viable. The proposed triangular electrode arrangements with copper material are very rich in generating low thermal gradient which regulates high temperature at the tip of electrode region rather than any other portion of the device in case of single run. Gold and platinum electrode material remain effective for many runs, as the main channel does not darken in this case. Thermal damage to cells using a triangular electrode is less than any other electrode geometry with a applied potential in range of 10V to 40V which makes it suitable to use in all electrode based dielectrophoretic devices. Hence, our proposed guidelines will enable the researcher to design microfluidic devices without relying on complex process in order to minimize the joule heating effect inside the microchannel. The proposed parameters are more efficient in collecting healthy cells at the outlet bins with minimized joule heating in all DEP based devices.

Conflicts of Interest: The authors declare no conflict of interest.

References

1. N.A. Rahman, F. Ibrahim, B. Yafouz, Dielectrophoresis for biomedical sciences applications: A review, *Sensors (Switzerland)*. **17 (2017)**.
2. H. Yan, H. Wu, Joule Heating and Chip Materials, in: Encycl. Microfluid. *Nanofluidics, Springer US*, **2014**: pp. 1–15.
3. M. Punjiya, H.R. Nejad, J. Mathews, M. Levin, S. Sonkusale, A flow through device for simultaneous dielectrophoretic cell trapping and AC electroporation, *Sci. Rep. 9* **(2019)**, pp.1–11.
4. G. Velve-Casquillas, M. Le Berre, M. Piel, P.T. Tran, Microfluidic tools for cell biological research, *Nano Today. 5* **(2010)**, pp.28–47.
5. A. Valero, T. Braschler, N. Demierre, P. Renaud, A miniaturized continuous dielectrophoretic cell sorter and its applications, *Biomicrofluidics. 4* **(2010)**.
6. T.M. Pearce, J.A. Wilson, S.G. Oakes, S.Y. Chiu, J.C. Williams, Integrated microelectrode array and microfluidics for temperature clamp of sensory neurons in culture, *Lab Chip. 5* **(2005)**, pp.97–101.
7. J. Wang, Y. Wei, S. Zhao, Y. Zhou, W. He, Y. Zhang, W. Deng, The analysis of viability for mammalian cells treated at different temperatures and its application in cell shipment, *PLoS One. 12* **(2017)**, pp.1–16.
8. S. Chen, Z. Wang, X. Cui, L. Jiang, Y. Zhi, X. Ding, Z. Nie, P. Zhou, D. Cui, Microfluidic Device Directly Fabricated on Screen-Printed Electrodes for Ultrasensitive Electrochemical Sensing of PSA, *Nanoscale Res. Lett. 14* **(2019)**, pp. 0–6.
9. L. Chen, X. Liu, X. Zheng, X. Zhang, J. Yang, T. Tian, Y. Liao, Dielectrophoretic separation of particles using microfluidic chip with composite three-dimensional electrode, *Micromachines. 11* **(2020)**.
10. G. Kunti, J. Dhar, A. Bhattacharya, S. Chakraborty, Joule heating-induced particle manipulation on a microfluidic chip, *Biomicrofluidics. 13* **(2019)**.
11. A. Kausar, R. Taherian, Effect of external fields on electrical conductivity of polymer-based composites, *Elsevier Inc.*, **(2018)**.
12. S.H. Song, B.S. Kwak, J.S. Park, W. Kim, H. IL Jung, Novel application of Joule heating to maintain biocompatible temperatures in a fully integrated electromagnetic cell sorting system, Sensors Actuators, *A Phys. 151* **(2009)**, pp.64–70.
13. B. Del Rosal, C. Sun, D.N. Loufakis, C. Lu, D. Jaque, Thermal loading in flow-through electroporation microfluidic devices, *Lab Chip. 13* **(2013)**, pp.3119–3127.

14. G.Y. Tang, D.G. Yan, C. Yang, H.Q. Gong, C.J. Chai, Y.C. Lam, Joule heating and its effects on electroosmotic flow in microfluidic channels, *J. Phys. Conf. Ser. 34* **(2006)**, pp.925–930.

15. J. Vlassakis, A.E. Herr, Joule Heating-Induced Dispersion in Open Microfluidic Electrophoretic Cytometry, *Anal. Chem. 89* **(2017)**, pp.12787–12796.

16. E.O. Adekanmbi, S.K. Srivastava, Dielectrophoretic applications for disease diagnostics using lab-on-a-chip platforms, *Lab Chip. 16* **(2016)**, pp.2148–2167.

17. D.R. Albrecht, R.L. Sah, S.N. Bhatia, Geometric and material determinants of patterning efficiency by dielectrophoresis, *Biophys. J. 87* **(2004)**, pp.2131–2147.

18. B.I.M.Z. Ansar, V. Tirth, C.M. Yousuff, N.K. Shukla, S. Islam, K. Irshad, K.O.M. Aarif, Simulation Guided Microfluidic Design for Multitarget Separation Using Dielectrophoretic Principle, *Biochip J. 14* **(2020)**, pp.390–404.

19. Z.T.F. Yu, K.M. Aw Yong, J. Fu, Microfluidic blood cell sorting: Now and beyond, *Small. 10* **(2014)**, pp.1687–1703.

20. M.H. Wang, W.H. Chang, Effect of electrode shape on impedance of single HeLa cell: A COMSOL simulation, *Biomed Res. Int. 2015* **(2015)**.

21. M.B. Fox, D.C. Esveld, A. Valero, R. Luttge, H.C. Mastwijk, P. V. Bartels, A. Van Den Berg, R.M. Boom, Electroporation of cells in microfluidic devices: A review, *Anal. Bioanal. Chem. 385* **(2006)**, pp.474–485.

22. M. Dewhirst, B.L. Viglianti, M. Lora-Michiels, P.J. Hoopes, M.A. Hanson, Thermal dose requirement for tissue effect: experimental and clinical findings, in: Therm. Treat. Tissue Energy Deliv. Assess. II, *SPIE,* **(2003)**, p. 37.

23. B. Sarno, D. Heineck, M.J. Heller, S. Ibsen, Dielectrophoresis: Developments and applications from 2010 to 2020, *Electrophoresis.* **(2020)**, pp.1–54.

24. R. Pethig, Dielectrophoresis: An assessment of its potential to aid the research and practice of drug discovery and delivery, *Adv. Drug Deliv. Rev. 65* **(2013)**, pp.1589–1599.

25. C.M. Yousuff, E.T.W. Ho, K. Ismail Hussain, N.H.B. Hamid, Microfluidic platform for cell isolation and manipulation based on cell properties, *Micromachines. 8* **(2017)**, pp.1–26.

26. M.Z. Rashed, N.G. Green, S.J. Williams, Scaling law analysis of electrohydrodynamics and dielectrophoresis for isomotive dielectrophoresis microfluidic devices, *Electrophoresis. 41* **(2020)**, pp.148–155.

27. M.-H. Wang, W.-H. Chang, Effect of Electrode Shape on Impedance of Single HeLa Cell: A COMSOL Simulation., *Biomed Res. Int. 2015* **(2015)**, pp.871603.

28. J. Zhang, Z. Song, Q. Liu, Y. Song, Recent advances in dielectrophoresis-based cell viability assessment, *Electrophoresis. 41* **(2020)**, pp.917–932.

29. R. Pethig, Dielectrophoresis: Status of the theory, technology, and applications, *Biomicrofluidics. 4* **(2010)**, pp.1–35.

30. C. Qian, H. Huang, L. Chen, X. Li, Z. Ge, T. Chen, Z. Yang, L. Sun, Dielectrophoresis for bioparticle manipulation, *Int. J. Mol. Sci. 15* **(2014)**, pp.18281–18309.

31. D. Erickson, D. Sinton, D. Li, Joule heating and heat transfer in poly(dimethylsiloxane) microfluidic systems, *Lab Chip. 3* **(2003)**, pp.141–149.

32. R. Chein, Y.C. Yang, Y. Lin, Estimation of Joule heating effect on temperature and pressure distribution in electrokinetic-driven microchannel flows, *Electrophoresis. 27* **(2006)**, pp.640–649.

33. O.T. Nedelcu, A thermal study on joule-heating induced effects in dielectrophoretic microfilters, *Rom. J. Inf. Sci. Technol. 14* **(2011)**, pp.309–323.

34. Y. Zhu, S. Nahavandi, A. Bui, K. Petkovic-Duran, Joule heating in polymer microfluidic chip, in: *BioMEMS Nanotechnol. II,* **(2005)**, pp. 603612

35. T. Brans, F. Strubbe, C. Schreuer, S. Vandewiele, K. Neyts, F. Beunis, Joule heating monitoring in a microfluidic channel by observing the Brownian motion of an optically trapped microsphere, *Electrophoresis. 36* **(2015)**, pp.2102–2109.

36. X.B. Wang, J. Yang, Y. Huang, J. Vykoukal, F.F. Becker, P.R.C. Gascoyne, Cell separation by dielectrophoretic field-flow-fractionation, *Anal. Chem. 72* **(2000)**, pp.832–839.

37. R.S.W. Thomas, P.D. Mitchell, R.O.C. Oreffo, H. Morgan, N.G. Green, Image-based sorting and negative dielectrophoresis for high purity cell and particle separation, *Electrophoresis. 40* **(2019)**, pp.2718–2727.

38. A. Salari, M. Navi, T. Lijnse, C. Dalton, AC electrothermal effect in microfluidics: A review, *Micromachines. 10* **(2019)**.pp. 1–27.

39. C.M. Yousuff, N.H.B. Hamid, K.I. Hussain, E.T.W. Ho, Numerical modelling and simulation of dielectrophoretic based WBC sorting using sidewall electrodes, in: *Int. Conf. Intell. Adv. Syst. ICIAS* **2016, 2017**: pp. 1–5.

40. H. Zhang, H. Chang, P. Neuzil, DEP-on-a-chip: Dielectrophoresis applied to microfluidic platforms, *Micromachines. 10* **(2019)**.

41. M.S. Jaeger, T. Mueller, T. Schnelle, Thermometry in dielectrophoresis chips for contact-free cell handling, *J. Phys. D. Appl. Phys. 40* **(2007)**, pp.95–105.

42. T. Jiang, Y. Ren, W. Liu, D. Tang, Y. Tao, R. Xue, H. Jiang, Dielectrophoretic separation with a floating-electrode array embedded in microfabricated fluidic networks, *Phys. Fluids. 30* **(2018)**.

43. H. Chen, B. Cao, B. Sun, Y. Cao, K. Yang, Y.S. Lin, H. Chen, Highly-sensitive capture of circulating tumor cells using micro-ellipse filters, *Sci. Rep. 7* **(2017)**, pp.1–10.

44. J. Fildes, S. Fisher, C.M. Sheaff, J.A. Barrett, Effects of short heat exposure on human red and white blood cells, *J. Trauma - Inj. Infect. Crit. Care. 45* **(1998)**, pp.479–484.

45. B.J. Wood, J.R. Ramkaransingh, T. Fojo, M.M. Walther, S.K. Libutti, Percutaneous tumor ablation with radiofrequency, *Cancer. 94* **(2002)**, pp.443–451.

46. S.H. Beachy, E.A. Repasky, Toward establishment of temperature thresholds for immunological impact of heat exposure in humans, *Int. J. Hyperth. 27* **(2011)**, pp.344–352.

47. S. McDermott, D.A. Gervais, Radiofrequency ablation of liver tumors, *Semin. Intervent. Radiol. 30* **(2013)**, pp.49–55..

48. M.Z. Ansar, M.Y. Caffiyar, A. Mohammed Kashif, Microfluidic device for Multitarget separation using DEP techniques and its applications in clinical research, in: 2020 6th Int. Conf. Bio Signals, Images, Instrumentation, *ICBSII 2020, Institute of Electrical and Electronics Engineers Inc.*, **(2020)**.

49. S. Sridharan, J. Zhu, G. Hu, X. Xuan, Joule heating effects on electroosmotic flow in insulator-based dielectrophoresis, *Electrophoresis. 32* **(2011)**, pp. 2274–2281

50. M. Kim, S. Mo Jung, K.H. Lee, Y. Jun Kang, S. Yang, A microfluidic device for continuous white blood cell separation and lysis from whole blood, *Artif. Organs. 34* **(2010)**, pp.996–1002.

51. C. Birch, J.P. Landers, Electrode materials in microfluidic systems for the processing and separation of DNA: A mini review, *Micromachines. 8* **(2017)**, pp.1–14.

52. Y. Yuan, K. Amine, J. Lu, R. Shahbazian-Yassar, Understanding materials challenges for rechargeable ion batteries with in situ transmission electron microscopy, *Nat. Commun. 8* **(2017)**, pp.1–14.

53. M.R. Haq, Y.K. Kim, J. Kim, J. Ju, S.M. Kim, Fabrication of all glass microfluidic device with superior chemical and mechanical resistances by glass molding with vitreous carbon mold, *J. Micromechanics Microengineering. 29* **(2019).**

54. D. Attinger, C. Frankiewicz, A.R. Betz, T.M. Schutzius, R. Ganguly, A. Das, C.-J. Kim, C.M. Megaridis, Surface engineering for phase change heat transfer: A review, *MRS Energy Sustain. 1* **(2014)**, pp.1–40.

55. J. Wei, M. Liao, A. Ma, Y. Chen, Z. Duan, X. Hou, M. Li, N. Jiang, J. Yu, Enhanced thermal conductivity of polydimethylsiloxane composites with carbon fiber, *Compos. Commun. ,17,* **(2020)**, pp.141–146.

56. I. Donmez Noyan, M. Dolcet, M. Salleras, A. Stranz, C. Calaza, G. Gadea, M. Pacios, A. Morata, A. Tarancon, L. Fonseca, All-silicon thermoelectric micro/nanogenerator including a heat exchanger for harvesting applications, *J. Power Sources. 413* **(2019)**, pp.125–133.

57. Z. Han, A. Fina, Thermal conductivity of carbon nanotubes and their polymer nanocomposites: A review, Prog. Polym. Sci. 36 (2011) 914–944. https://doi.org/10.1016/j.progpolymsci.2010.11.004.

58. T.H.N. Dinh, E. Martincic, E. Dufour-Gergam, P.Y. Joubert, Mechanical characterization of PDMS films for the optimization of polymer based flexible capacitive pressure microsensors, *J. Sensors.* **(2017)**.

59. R.I. Acosta, K.C. Gross, G.P. Perram, Thermal degradation of Poly(methyl methacrylate) with a 1.064 μm Nd:YAG laser in a buoyant flow, *Polym. Degrad. Stab. 121* **(2015)**, pp.78–89.

60. S. Sathya, M. Pavithra, S. Muruganand, Simulation of Electrostatic Actuation in Interdigitated Comb Drive MEMS Resonator for Energy Harvester Applications, *IOP Conf. Ser. Mater. Sci. Eng. 149* **(2016).**

61. S. Halldorsson, E. Lucumi, R. Gómez-Sjöberg, R.M.T. Fleming, Advantages and challenges of microfluidic cell culture in polydimethylsiloxane devices, Biosens. Bioelectron. 63 **(2015)**, pp.218–231.

62. A.L. Paguirigan, D.J. Beebe, From the cellular perspective: Exploring differences in the cellular baseline in macroscale and microfluidic cultures, *Integr. Biol. 1* **(2009)**, pp.182–195

63. R.R. Richardson, J.A. Miller, W.M. Reichert, Polyimides as biomaterials: preliminary biocompatibility testing, *Biomaterials.* **14 (1993)**, pp. 627–635.

64. C.P. Constantin, M. Aflori, R.F. Damian, R.D. Rusu, Biocompatibility of polyimides: *A mini-review, Materials (Basel).* **12 (2019)**.

65. U. Ali, K.J.B.A. Karim, N.A. Buang, A Review of the Properties and Applications of Poly (Methyl Methacrylate) (PMMA), *Polym. Rev. 55* **(2015),** pp. 678–705.

66. V. Gill, P.R. Guduru, B.W. Sheldon, Electric field induced surface diffusion and micro/nano-scale island growth, *Int. J. Solids Struct.* 45 **(2008)**, pp.943–958.